MWCNTs decorated with $Mn_{0.8}Zn_{0.2}Fe_2O_4$ nanoparticles for removal of crystal-violet dye from aqueous solutions

M.A. Gabal [a,*], E.A. Al-Harthy [a,b], Y.M. Al Angari [a], M. Abdel Salam [a]

[a] Chemistry Department, Faculty of Science, King Abdulaziz University, Jeddah, Saudi Arabia
[b] Center of Excellence in Environmental Studies, King Abdulaziz University, PO Box 80216, Jeddah 21589, Saudi Arabia

HIGHLIGHTS

- $Mn_{0.8}Zn_{0.2}Fe_2O_4$ was prepared using spent Zn–C batteries through sucrose method.
- MWCNTs/$Mn_{0.8}Zn_{0.2}Fe_2O_4$ nano-composite was prepared via same method.
- The nano-composite was characterized and investigated to remove crystal violet dye.
- After removal, the nano-composite can be easily separated using a normal magnet.
- The optimum condition for the efficient removal was investigated and discussed.

GRAPHICAL ABSTRACT

TEM image showed that MWCNTs are homogeneously decorated with $Mn_{0.8}Zn_{0.2}Fe_2O_4$ particles. The interaction seems to be sufficiently strong, as demonstrated by the absence of any free ferrite particles especially after prolonged sonication subsequent to TEM measurement.

ARTICLE INFO

ABSTRACT

In the present study, a simple, economic and environmentally friend method was utilized for the production of multi-walled carbon nanotubes (MWCNTs) decorated with $Mn_{0.8}Zn_{0.2}Fe_2O_4$ nanoparticles, synthesized via recycling process of Zn–C battery. The chemical composition and structure of the MWCNTs/$Mn_{0.8}Zn_{0.2}Fe_2O_4$ composite were confirmed by X-ray diffraction and Fourier transform infrared measurements. The morphology as well as the decoration process was characterized using transmission electron microscopy. The results showed that the MWCNTs are homogeneously decorated with cubic loosely agglomerated ferrite particles having mean crystallite size of 20 nm. An appropriate decoration mechanism was suggested and discussed. The hysteresis measurements exhibited reasonable magnetic characteristics for the obtained composite which facilitate its separation from their dispersed solution using normal magnet. Surface area measurement indicates relatively large specific surface enhances its use in adsorption process. The adsorption capacity of the entire composite was investigated using crystal violet dye. The effect of composite mass, contact time, solution pH and solution temperature on the adsorption process was investigated. The adsorption process was found to follow a pseudo-second-order model. The calculated adsorption thermodynamic parameters (ΔG, ΔH and ΔS) suggested the spontaneity of the thermodynamically favorable adsorption process.

© 2014 Elsevier B.V. All rights reserved.

* Corresponding author. Permanent address: Chemistry Department, Faculty of Science, Benha University, Benha, Egypt. Tel.: +20 00966557071572.
E-mail address: mgabalabdonada@yahoo.com (M.A. Gabal).

1. Introduction

Due to their unique structure, carbon nanotubes (CNTs) were found to exhibit many fascinating characteristics including mechanical, electronic and chemical properties [1,2]. Recently, they have been investigated as a promising adsorbent for many organic and inorganic pollutants depending on their large surface area, fibrous shape and layered structure [3–5]. The adsorption capacity can be easily modified through chemical treatment with some metal oxides [6,7]. In this category, unique magnetic characteristics can be obtained through magnetic modification of CNTs with iron oxides [8] as well as some ferrite materials [3], which enhances their uses as magnetic data storage [9], microwave-absorbing materials [10], magnetic composites for drug delivery [11], etc. besides their uses as adsorbents [12].

Many researchers in the literature were reported on the synthesis and characterization of multi-walled carbon nanotubes (MWCNTs)/ferrite nano-composite used for different applications [13–17] but on the other hand, very few works dealing with the adsorption capability of these nano-composites are presented.

Farghali et al. [18] presented a simple hydrothermal precipitation method for producing MWCNTs decorated with $CoFe_2O_4$ nanoparticles used to investigate the adsorption capability of methylene blue dye.

Abdel Salam et al. [12] synthesized MWCNTs/$NiFe_2O_4$ nano-composite and used it for the removal of aniline from aqueous solution.

Zhang et al. [16] synthesized $Mn_{1-x}Zn_xFe_2O_4$/MWCNTs ($0 < x < 1$) via solvothermal method. The obtained composites were characterized by XRD, TEM, SEM and vibrating sample magnetometry (VSM). An appropriate mechanism for the nano-composite formation was also investigated. To the best of our knowledge, this is the only work in the literature dealing with MWCNTs/Mn–$ZnFe_2O_4$ nano-composite. In the present work, we prepared similar nano-composite via an alternative simple, cheap, economic and environmentally friend method using sucrose [19]. The contents of the entire ferrite, viz. manganese, zinc and iron will be obtained through recycling process of Zn–C battery previously described [20]. The prepared nano-composite will be characterized and investigated to remove crystal violet (CV) dye from aqueous solutions as an example of organic pollutants.

2. Experimental

2.1. Preparation of the MWCNTs/ferrite magnetic nano-composite

MWCNTs with average diameters of 60–100 nm were obtained from Shenzhen Nano-Technologies, China, and were used as received.

A recycling process of Zn–C battery was carried out, as previously described [20] to extract Mn, Zn and Fe required for ferrite preparation. Then, the stoichiometric ratios of each metal to prepare $Mn_{0.8}Zn_{0.2}Fe_2O_4$ were achieved using analytical reagents metal nitrates. The procedure for the preparation of entire ferrites using sucrose method is followed as previously reported in [19]. Stoichiometric amounts of metal nitrates in 100 ml distilled water and sucrose aqueous solution (12 g dissolved in 50 ml distilled water) are mixed thoroughly and kept at 60 °C for 30 min under vigorous stirring. The pH was adjusted to 7 by the addition of ammonia solution. The sticky gel obtained was evaporated until the combustion process occurs. The obtained loose as-prepared powder was then grounded and stored in dessicator.

MWCNTs/ferrite magnetic nano-composite (containing 70% w/w MWCNTs) was prepared by thoroughly mixing of MWCNTs with the stoichiometric amount of the entire metal nitrates during the preparation of the respective ferrite nanoparticles. The suspension

obtained was then subjected for 1 h sonication process after which the same above procedures are followed until obtaining nano-composite.

2.2. Characterization techniques

The chemical composition of the battery contents was determined using atomic absorption spectrophotometer (AAS). The crystal phase was characterized by XRD using a Bruker axs D8 high-resolution diffractometer employing Cu-Kα radiation ($\lambda = 0.15418$ nm). The morphology was characterized by transmission electron microscopy using a JEOL-2010 instrument running at an accelerating voltage of 100 kV. Fourier transform infrared spectra were measured using a FT-IR, Perkin–Elmer in the range of 600–200 cm^{-1} using KBr-pellet technique. Magnetic properties were measured at room temperature using a vibrating sample magnetometer (VSM-9600 M) at applied magnetic field up to 5 kOe. The specific surface area was determined from nitrogen adsorption/desorption isotherms measured at 77 K using a model NOVA 3200e automated gas sorption system (Quantachrome, USA).

2.3. Adsorption experiment

Adsorption experiments were performed to determine the effect of the MWCNTs/ferrite magnetic nano-composite mass, solution pH, time and temperature on the adsorption process. The experimental procedures were performed as follows: (1) 20 ml of 10.0 mg L^{-1} solution of CV was prepared; (2) the initial pH was measured, and a defined amount of the magnetic nano-composite was then added to the solution; (3) these solution was stirred on a magnetic stirrer for a certain period of time, at room temperature; (4) at definite time intervals, a certain volume of the solution was removed and immediately using ordinary magnet the clear supernatant was collected using a glass pasture pipette; and (5) the residual CV concentration in the supernatant was determined using Perkin Elmer Lambda 25 UV–Vis spectrophotometer, USA at wavelength 588 nm. The amount of CV removed was determined by measuring the difference in the concentrations of the samples that were obtained at two consecutive time intervals over the course of the adsorption experiment using the following equation:

$$\% \text{ Crystal Violet Removed} = 100 - \frac{C_t}{C_0} \times 100 \qquad (1)$$

where C_0 and C_t are the concentrations of CV in solution (mg L^{-1}) at time $t = 0$ and t, respectively.

2.4. Real water samples collection

The efficiency and applicability of MWCNTs/ferrite magnetic nano-composite for the removal of CV was explored using real water samples. A tap water sample (TWS); collected from our lab after allowing the tap water to flow for 10 min, and a wastewater sample, collected from the Waste Water Treatment Plant (Membrane Bio-Reactor Technology) – King Abdulaziz University (KAUWW), Jeddah City (Latitude deg. North 21.487954, Longitude deg. East 39.236748). Both samples were filtered through 0.45 μm Millipore filter paper and kept in Teflon® bottles at 5 °C in the dark.

3. Results and discussion

3.1. Characterization of MWCNTs/ferrite magnetic nano-composite

3.1.1. X-ray diffraction

Fig. 1 shows XRD patterns of the as-prepared $Mn_{0.8}Zn_{0.2}Fe_2O_4$, using Zn–C battery extract, and MWCNTs/$Mn_{0.8}Zn_{0.2}Fe_2O_4$ compo-

site. The appearance of the diffraction peaks corresponds to $(1\,1\,1)$, $(2\,2\,0)$, $(3\,1\,1)$, $(2\,2\,2)$, $(4\,0\,0)$, $(4\,2\,2)$, $(5\,1\,1)$ and $(4\,4\,0)$ crystal planes, in consistent with the database found in the JCPDS file No. 74-2402, indicate the formation of single-phase cubic $Mn_{0.8}Zn_{0.2}Fe_2O_4$. The observed diffraction peak appeared around 26°, corresponds to the graphite $(0\,0\,2)$ plane of CNTs [21], which confirms the retaining of CNTs structure without any destruction.The broadness of the diffraction peaks indicated the nano-crystallinity of the samples. The average sizes of the pure $Mn_{0.8}Zn_{0.2}Fe_2O_4$ and when coated on MWCNTs, were calculated using the Debye–Scherrer formula [22] and are found to be 39.5 and 17.9 nm, respectively. This obvious decrease in the size on coating can be attributed to the adsorption of the entire ions on the surface of CNTs during sonication process. This spreading on the surface can be consequently prevented the accumulation of particles during the combustion process and ferrite formation.

The values of the lattice parameter calculated using the interplanar distance (d) along with peaks reflections according to the Bragg's equation [22] exhibited an obvious decrease from 8.4359 Å for pure ferrite to 8.4039 Å after coating. This behavior agrees well with the decrease in the particle size previously described. In addition, the observed increase in the calculated density from 5.15 to 5.21 g cm^{-3} on coating can also be attributed to the size change.

3.1.2. TEM images

TEM images of $Mn_{0.8}Zn_{0.2}Fe_2O_4$, MWCNTs as well as their composite are represented in Fig. 2. The image of the entire ferrite (Fig. 2a) exhibited regularly shaped cubic agglomerated particles with size of about 40 nm. The agglomeration behavior of the particles can be due to the magnetostatic interaction between magnetic particles or the experience of the nanoparticles for a permanent magnetic moment proportional to their volume [23]. MWCNTs image (Fig. 2b) showed micro-sized tubes with a diameter of about 20 nm.

Fig. 2c exhibited the interaction between $Mn_{0.8}Zn_{0.2}Fe_2O_4$ and MWCNTs. From this image, it is clear that most of the MWCNTs are homogeneously decorated with ferrite particles. The ferrite particles appeared to be loosely agglomerated and exhibited regularly shaped cubic particles with mean crystallite size of 20 nm, which is smaller than that of the original ferrite. The interaction seems to be sufficiently strong, as demonstrated by the absence of any free ferrite particles especially after prolonged sonication subsequent to TEM measurement. Generally, the obtained sizes via TEM measurements agrees well with those obtained previously using XRD measurements.

3.1.3. FT-IR spectroscopy

FT-IR spectrum of pure MWCNTs as well as MWCNTs/$Mn_{0.8}Zn_{0.2}Fe_2O_4$ nano-composite is illustrated in Fig. 3. As can be seen from comparing the two spectrums all the bands appeared above 800 cm^{-1} can be assigned to MWCNTs. The two broad bands observed in the range 400–600 cm^{-1} can be assigned according to Waldron [24] to the oxygen–metal absorption bands of spinel structure, especially ferrites. The higher frequency band appeared at 567 cm^{-1} can be corresponded to the intrinsic stretching vibrations of the metal at the tetrahedral site, while the lower frequency band at 449 cm^{-1} can be ascribed to the octahedral-metal stretching.

3.1.4. Magnetic properties

The magnetic properties of the uncoated MWCNTs and coated with $Mn_{0.8}Zn_{0.2}Fe_2O_4$ as well as the as-prepared ferrite were measured by VSM, as shown in Fig. 4. From the figure, different magnetic parameters such as saturation magnetization (M_s), coercivity (H_c) and remnant magnetization (M_r) were estimated and given in Table 1.

The magnetization value of the entire ferrite is observed to be significantly higher than that of the bulk ferrite (M_s = 45 emu/g) [19]. On coating, the saturation magnetization of the composite was lowered to 28 emu/g, which can be attributed mainly to the contribution of the magnetization of the weak-magnetic MWCNTs to the total composite magnetization. The inset of Fig. 4 showed that these magnetic MWCNTs could be easily separated from their dispersed solution by using a normal magnet. This indicates the high magnetic sensitivity of our nano-composite besides its high surface area, which enhances its use in the remediation applications.

3.2. Decoration mechanism and composite formation

The proposed mechanism for the decoration process and nano-composite formation is shown in Fig. 5. On soaking MWCNTs in the metal nitrates solution and during the sonication process, the entire metals tend to adsorb on the surface of MWCNTs. As previously described [19], in the sucrose auto-combustion process, the metal nitrates are acting as oxidizing agents while sucrose acts as a fuel. Under the entire experimental conditions, in the presence of H$^+$ from nitric acid, the sucrose can be hydrolyzed to glucose and fructose, which can be further oxidized into saccharic acid, glycolic acid and trihydroxy-butyric acid with a number of –COOH and –OH groups [25,26] and in this case, sucrose can be functioned as a complexing agent for the entire metal ions. On adjusting pH of solution to about 7 a polyesterification reaction was promoted with the formation of viscous resin complex [27]. On successive heating and at the point of spontaneous combustion, the sticky gel constituents were decomposed with the evolution of dense gases which make the gel to expand more than 10 times with the formation of highly porous ferrites. The combustion reaction can be written as follows [19]:
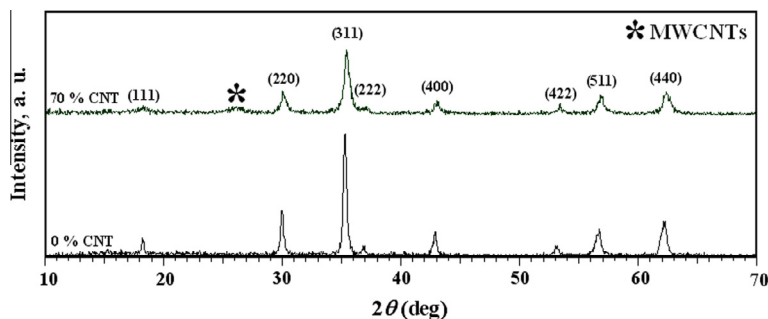
Fig. 1. XRD patterns of (a) $Mn_{0.8}Zn_{0.2}Fe_2O_4$ and (b) MWCNTs/$Mn_{0.8}Zn_{0.2}Fe_2O_4$ nano-composite.
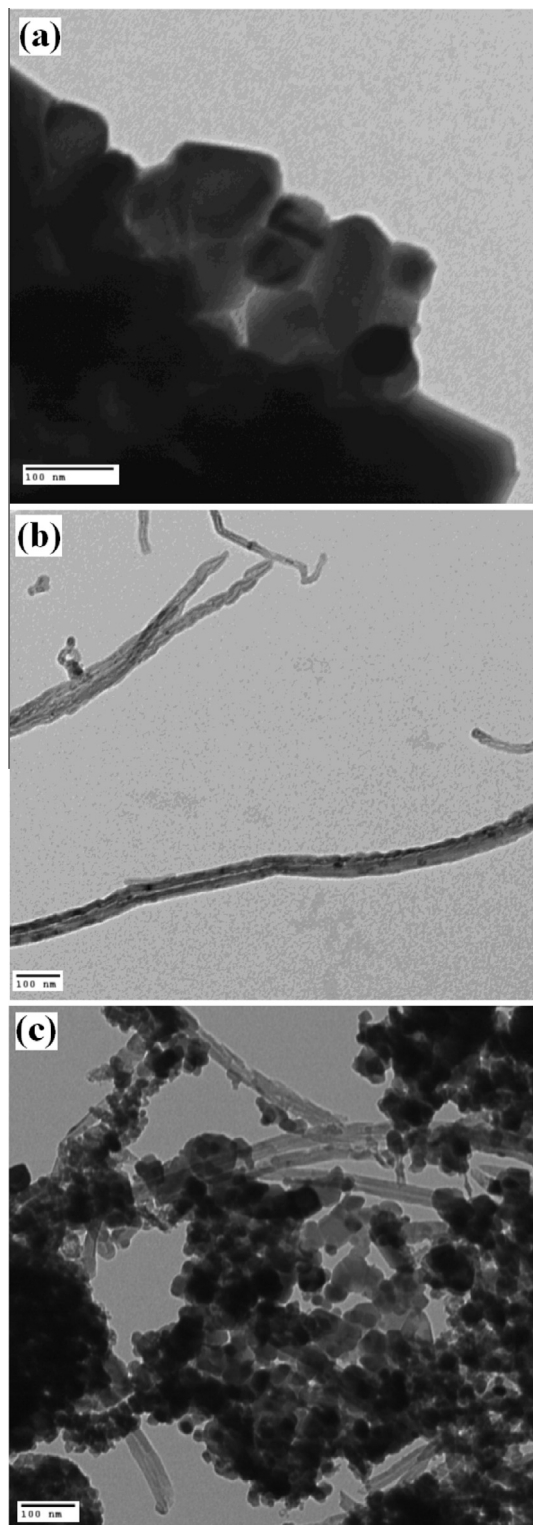
Fig. 2. TEM images of: (a) $Mn_{0.8}Zn_{0.2}Fe_2O_4$, (b) MWCNTs and (c) $Mn_{0.8}Zn_{0.2}Fe_2O_4$/MWCNTs nano-composite. Scale bar: 100 nm.

$$0.8Mn(NO_3)_2 \cdot 4H_2O + 0.2Zn(NO_3)_2 \cdot 6H_2O + 2Fe(NO_3)_3 \cdot 9H_2O$$
$$+ C_{12}H_{22}O_{11} + 2O_2$$
$$\rightarrow Mn_{0.8}Zn_{0.2}Fe_2O_4 + 12CO_2 + 4N_2 + 33.4H_2O$$
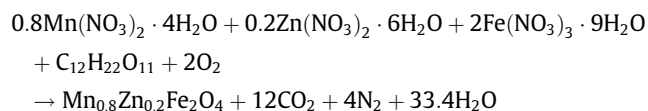
Finally, MWCNTs are coated by ferrite nanoparticles and form MWCNTs/$Mn_{0.8}Zn_{0.2}Fe_2O_4$ nano-composite.
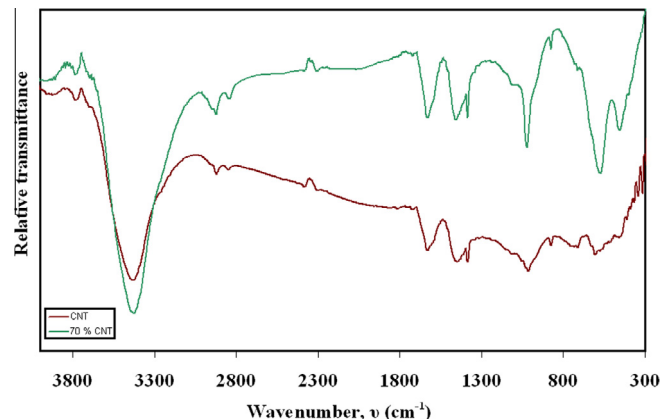
Fig. 3. FT-IR spectra of pure MWCNTs and $Mn_{0.8}Zn_{0.2}Fe_2O_4$/MWCNTs nano-composite.
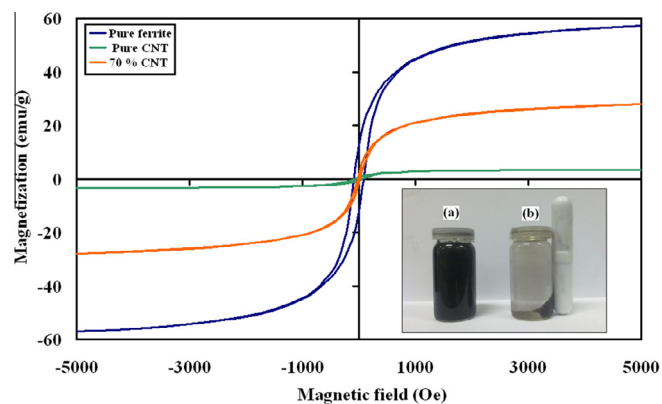
Fig. 4. Magnetic hysteresis loops for MWCNTs, $Mn_{0.8}Zn_{0.2}Fe_2O_4$ and $Mn_{0.8}Zn_{0.2}Fe_2O_4$/MWCNTs nano-composite. Inset: photograph of MWCNTs/$Mn_{0.8}Zn_{0.2}Fe_2O_4$ nano-composite (a) dispersed in water (b) its response to a magnet.

Table 1
Magnetic characteristics of MWCNTs, $Mn_{0.8}Zn_{0.2}Fe_2O_4$ and $Mn_{0.8}Zn_{0.2}Fe_2O_4$/MWCNTs nano-composite.

Materials	M_s (emu g^{-1})	H_c (Oe)	M_r (emu g^{-1})
$Mn_{0.8}Zn_{0.2}Fe_2O_4$	57.2	79.0	12.6
MWCNTs	3.4	54.3	0.5
MWCNTs/$Mn_{0.8}Zn_{0.2}Fe_2O_4$ nano-composite	28.0	18.7	1.4

3.3. Adsorption study

3.3.1. Surface area measurement

The specific surface areas and pore sizes distribution of the entire nano-composite were characterized using BET technique. The obtained results are illustrated in Fig. 6. According to the IUPAC classifications [28] the obtained adsorption/desorption isotherm (Fig. 6a) agrees well in behavior to type II isotherm. This type describes the adsorption on macroporous adsorbents accompanied by strong adsorbate–adsorbent interactions and exhibits a very small hysteresis behavior. The specific surface area calculated using the BET equation amounts to 59.8 m^2 g^{-1}. This value is relatively smaller than other previously reported for magnetic CNT materials [29] but is expected to be enough for enhancing the adsorption of CV dye. The pore sizes distribution estimated using Bareett–Joyner–Halenda (BJH) analysis (Fig. 6b) showed a pore size
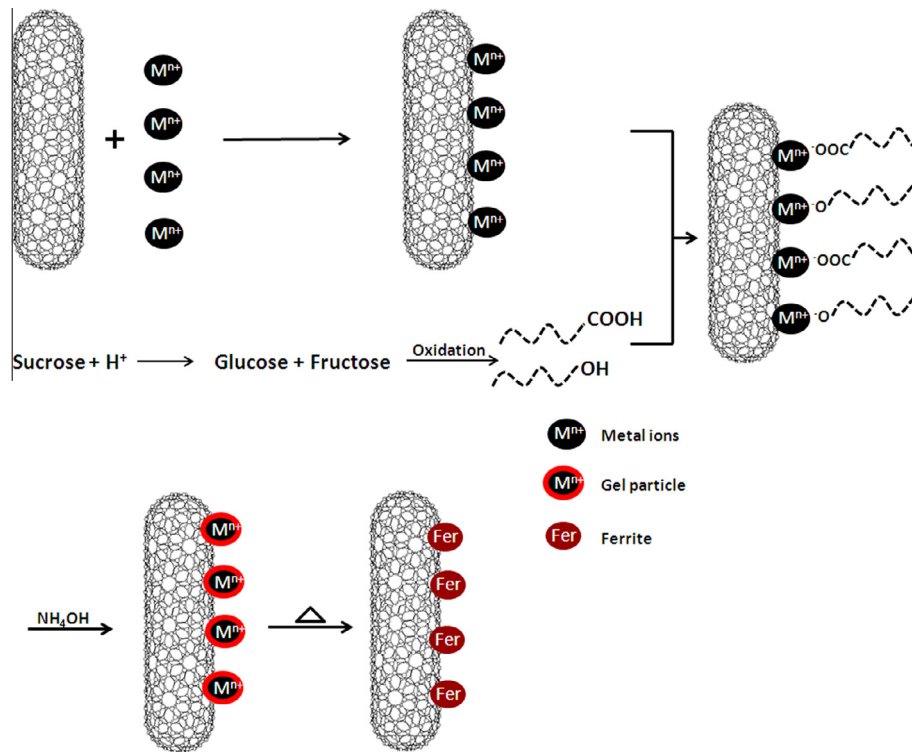
Fig. 5. Expected decoration mechanism.

of 1.5–3.0 nm. This corresponding small value can be attributed to the coating of CNT by ferrite.

3.3.2. Adsorption/removal of crystal violet (CV)

The adsorption capacity of MWCNTs/$Mn_{0.8}Zn_{0.2}Fe_2O_4$ nano-composite was examined via studying the adsorption/removal of CV dye from aqueous media. A certain amount of nano-composite was added to the CV solution and collected after a period with magnet and the concentration of CV removed was calculated. In this category, different parameters, which affected the removal process such as the mass of the solid adsorbent, solution temperature and pH, and the contact time between the adsorbent and the adsorbate were, studied (Fig. 7).

The effect of the adsorbent mass usually determines the solid adsorbent's capacity for a given initial concentration of adsorbate in a solution. Fig. 7a shows the effect of the nano-composite mass on the adsorption of CV from an aqueous solution (Experimental condition: at solution pH 8.0, 120 min, solution temperature 298 K, and CV concentration 10 mg L^{-1}). It is clear from the figure that the % CV removed increased gradually as the nano-composite mass increased, until it reached 88% when 50 mg of nano-composite was employed. This enhancement in the % CV removed principally due to the increase in the active sites on the nano-composite available for adsorption of CV molecules. Further increase in the dosage of nano-composite to 70 mg accompanied by further increase in the % CV removed to 100%.

Further experiments were conducted using 50 mg nano-composite to be able to observe the changes in the % CV removed from solution. Fig. 7b shows the effect of contact time on the adsorption of CV from an aqueous solution (Experimental conditions: 50 mg nano-composite, 20 ml sample, pH 8.0, 298 K, and CV concentration 10 mg L^{-1}). As it is clear from the figure, % CV removed increased gradually with increasing the contact time, till almost 75% of the CV removed within the first 30 min. Further increase in the contact time accompanied with slow increase in the% CV removed till it reached 91.0% after 120 min. The

experiment time was extent to 240 min and it was observed that most of the CV was removed after 150 min; 95% was removed. This may indicated that the adsorption start very fast on the external surface followed by a slower adsorption on the internal surface of the nano-composite.

The solution pH plays important role on the removal of CV from aqueous solution because the dye is very sensitive to the pH condition. Fig. 7c presented the obtained data for the removal capacity of the entire nano-composite over a pH range from 2 to 11 (Experimental conditions: 50 mg nano-composite, 20 ml sample, 120 min contact time, 298 K, and CV concentration 10 mg L^{-1}). Generally, it can be observed that % CV removed was enhanced by increasing solution pH. At a pH value of 2.0, the % removed was 76.8%, which increased to 84.7% at pH value of 8.0, then increased to 100% at a pH value of 11.0. This observed change may be due to the decrease in the charge density of the dye solution as a result of increasing pH, which greatly enhanced the electrostatic attraction between the positively charged CV molecules and the negatively charged nano-composite surface [30,31].

3.3.3. Kinetic studies

Adsorption kinetics is the study of the adsorption process rate to understand the factors that affect the adsorption process to attain equilibrium in a reasonable length of time. The effect of time on the removal CV from an aqueous solution by nano-composite was studied kinetically at different temperature and the results were presented in Fig. 8. In general, the CV removal was slightly enhanced by rising the solution temperature, and more importantly, the time required to reach equilibrium was decreased. The equilibrium time was decreased from 120 min, to 45 min, and 30 min, at 298 K, 313 K, and 328 K, respectively. This may indicated the endothermic nature of the removal of CV by nano-composite.

Kinetic studies usually use mathematical models to describe the interactions between the adsorbent and the adsorbate. The most frequently used kinetic models are the pseudo-first-order [32]
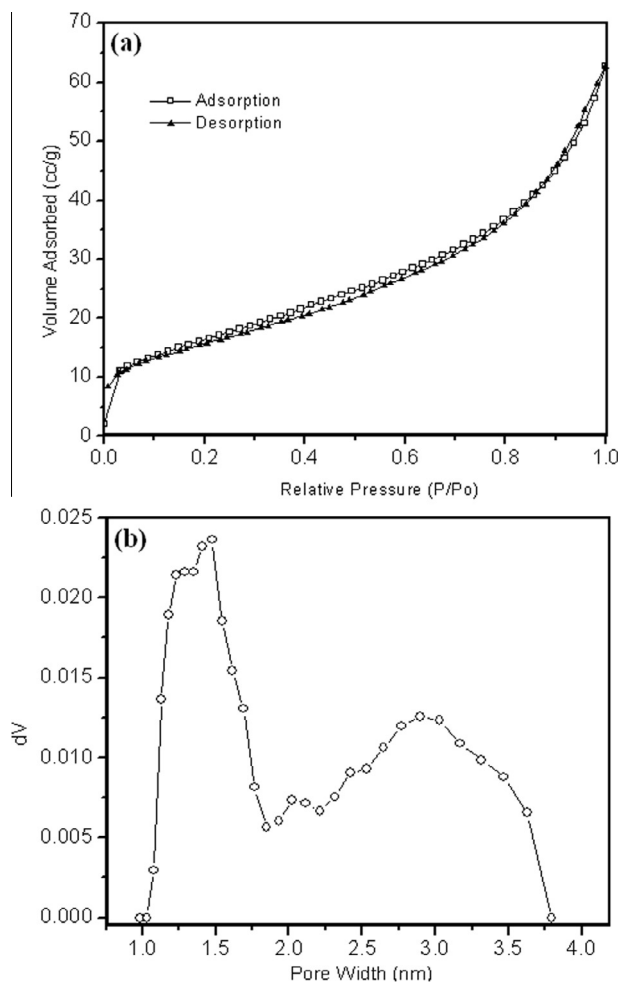
Fig. 6. (a) N$_2$ adsorption–desorption isotherm and (b) pore size distributions of MWCNTs/Mn$_{0.8}$Zn$_{0.2}$Fe$_2$O$_4$ nano-composite.

and pseudo-second-order kinetic models [33]. The linearized rate equations for both models are:

$$\ln (q_e - q_t) = \ln q_e - k_t \tag{2}$$

$$\frac{t}{q_t} = \frac{1}{k_2 q_e^2} + \frac{1}{q_e} \tag{3}$$

where k_1 and k_2 are the pseudo-first-order and pseudo-second-order adsorption rate coefficients, respectively and q_e and q_t are the values of the amount adsorbed per unit mass at equilibrium and at any time t, respectively.

Plotting $\ln (q_e - q_t)$ vs. t for the experimental data at different temperatures gave straight lines with unacceptable regression coefficients (Table 2), indicating the unsuitability of the pseudo-first-order for modeling the adsorption of the CV by nano-composite. On the other hand, by applying of the pseudo-second-order kinetic model, the plotting of t/q_t versus t (Fig. 9) give a linear relationship, with excellent regression coefficients ($R^2 > 0.99$), from which q_e and k_2 were estimated from the slope and intercept, respectively (Table 2). Also, the table shows that the amounts CV adsorbed per unit mass of nano-composite at equilibrium ($q_{e,\text{calc}}$) were in good agreement with experimental values ($q_{e,\text{exp}}$). These findings confirm the suitability of the pseudo-second-order rate equation for modeling the adsorption of CV by nano-composite.

According to the present study, the maximum adsorption capacity of CV by nano-composite obtained from an aqueous solution is 5.0 mg g^{-1} (Table 2). This value is much higher than the other
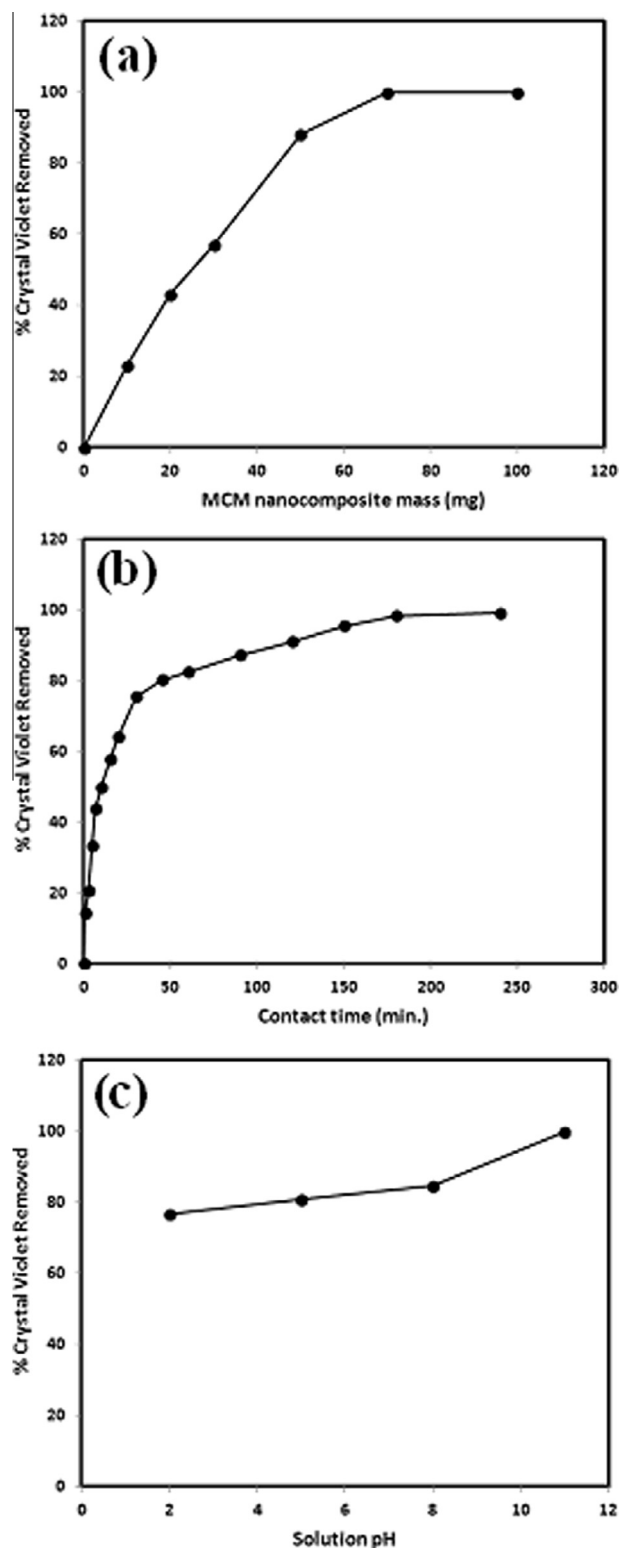
Fig. 7. (a) Effect of nano-composite mass (b) effect of contact time and (c) effect of pH on the % crystal violet removed.

adsorbents that are used for the removal of CV from aqueous solutions. For example, different nano-composite hydrogels with various clay contents were evaluated as a potential adsorbent for the removal of CV from aqueous solutions and the adsorption capacities were in the range 2.74–4.71 mg g^{-1} after 12 h [34]. In another study [35], soil-silver nano-composite was used for the removal of CV, and the adsorption capacity was 1.918 mg g^{-1} for
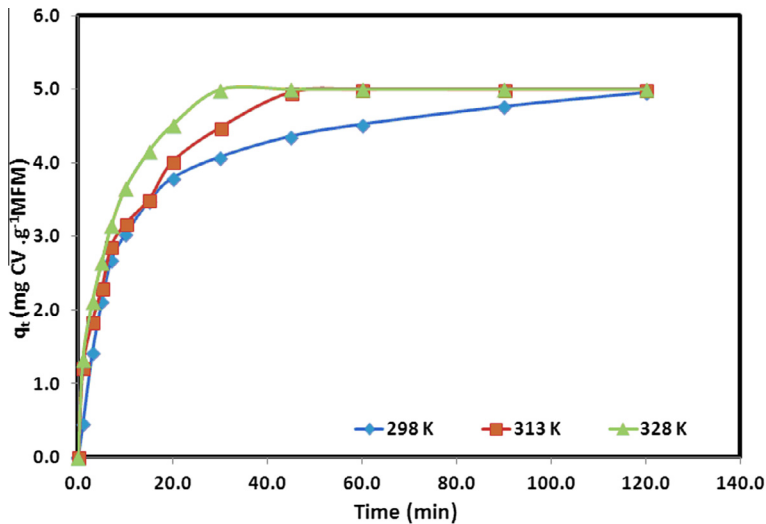
Fig. 8. Effect of temperature on the removal of CV. (Experimental conditions: 100 mg nano-composite, 100 ml sample volume, pH 8.0, and CV concentration 5 mg L^{-1}).

Table 2
Pseudo-first-order, and pseudo-second-order kinetic models parameters for the adsorption of crystal violet by nano-composite at different temperatures.

R^2	k_1	$q_{e,calc}$ (mg/g)	$q_{e,exp}$ (mg/g)	Temperature (K)
Pseudo-first-order kinetic model				
0.959	0.034	3.34	5.00	298
0.883	0.069	3.12	5.00	313
0.764	0.093	1.68	5.00	328
Pseudo-second-order kinetic model				
0.996	0.028	5.15	5.00	298
0.997	0.040	5.23	5.00	313
0.999	0.065	5.17	5.00	328

monolayer coverage. Also, in another study [36] the adsorption capacities for the removal of CV were 2.56 mg g^{-1} using coir pitch, 4.14 mg g^{-1} using Calotropis procera leaf and 6.25 mg g^{-1} using coal.

On the other hand, there were many studies reported substantial higher adsorption capacities compared with the present work, such as activated sintering process red mud (12.0 mg g^{-1}) [37] and powdered mycelial biomass of Ceriporia lacerate (239 mg g^{-1}) [38].

3.3.4. Thermodynamic studies

Thermodynamic parameters; Gibbs free energy change (ΔG), enthalpy change (ΔH) and, entropy change (ΔS), were calculated to explore the spontaneous nature of the adsorption process. Thermodynamic parameters were calculated from the variation of the thermodynamic distribution coefficient D with a change in temperature according to the equation [39]:

$$D = \frac{q_e}{C_e} \tag{4}$$

where q_e is the amount of CV adsorbed per unit mass of nano-composite (mg/g) at equilibrium, and C_e is the equilibrium concentration of CV in solution (mg/L). The ΔH and ΔS could be calculated according to the following equation [40,41]:

$$\log D = \frac{\Delta S}{R} - \frac{\Delta H}{2.303RT} \tag{5}$$

The plotting of *log D* vs. 1/*T* (Fig. 10) exhibited straight lines from which ΔH and ΔS values were calculated from the slope and the intercept of the straight line, respectively. The ΔG values were calculated at 298 K from the relation:

$$\Delta G = \Delta H - T\Delta S \tag{6}$$
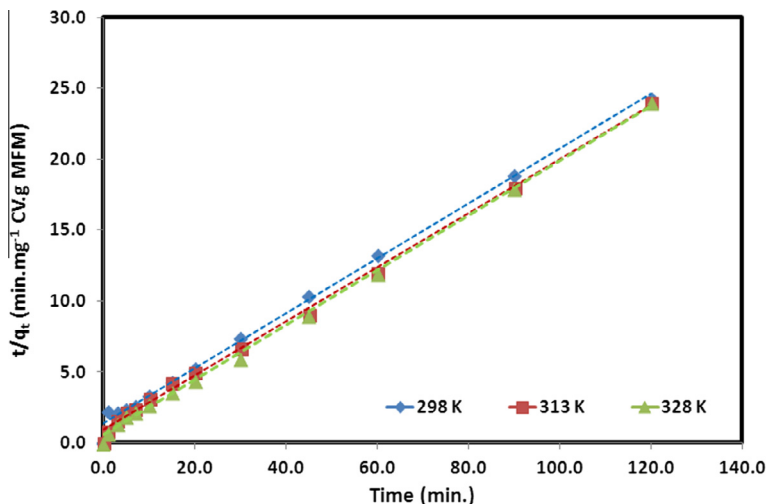
Fig. 9. Pseudo-second-order plots for the removal of CV by nano-composite at different temperatures. (Experimental conditions: 100 mg nano-composite, 100 ml sample volume, pH 8.0, and CV concentration 5 mg L^{-1}).
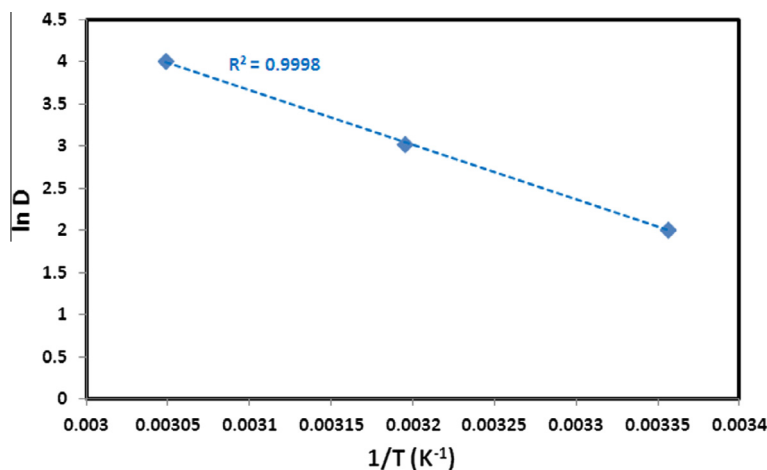
Fig. 10. Effect of temperature on the distribution coefficient (D) of crystal violet adsorbed by nano-composite.

The obtained free energy change (ΔG), according to the above equations, is amounted to -11.4 kJ/mole, which indicates the spontaneity of the adsorption process. The positive value obtained for ΔH (124.4 kJ/mole) verifying the endothermic nature of adsorption and suggests a strong type of bonding between the CV and nano-composite. The positive value obtained for ΔS (455.8 J/mol K), suggested the increase in the degree of freedom at the solid–liquid interface. Generally, the adsorption process was entropy driven process.

3.3.5. Environmental applications

Finally, real water samples were used to study the feasibility and applicability of the entire nano-composite for the adsorption/removal of the CV. The concentration of the CV was measured first on TWS and KAUWW samples and the results indicated the absence of the CV in both real water samples. Accordingly, the two real water samples were spiked with concentrated CV solution to obtain final concentration of 10.0 mg L^{-1} for both real water samples, and both solutions left over night to equilibrate. Then, 70 mg of the nano-composite was added to the spiked real water samples at pH 8.0, 298 K, for 120 min. The% CV removed was found to be 99.2% and 98.1% for the TWS and KAUWW, respectively. These values agreed very well with those obtained in the model solution as the% CV removed was 100%, under the same experimental conditions.

4. Conclusions

Multi-walled carbon nanotubes (MWCNTs) were successfully decorated with magnetic Mn$_{0.8}$Zn$_{0.2}$Fe$_2$O$_4$ using simple sucrose method. The synthesized nano-composite was characterized using XRD, FT-IR, TEM, BET and VSM techniques to explore its structure, morphology and magnetic properties. The magnetic measurements indicated that the nano-composite could be easily separated from their dispersed solution using a normal magnet, which enhance its uses in the remediation applications depending on its surface properties. The adsorption/removal experiments for the crystal violet dye from aqueous solution, as an example, using the entire nano-composite was found to be greatly depending on mass, contact time, pH and temperature. The optimum condition for the efficient removal was investigated and discussed.

Acknowledgements

References

[1] S.J. Tans, A.R.M. Verschueren, C. Dekker, Room-temperature transistor based on a single carbon nanotube, Nature 393 (1998) 49–52.

[2] Z.M. Dang, L.Z. Fan, Y. Shen, C.W. Nan, Dielectric behavior of novel three-phase MWNTs/BaTiO$_3$/PVDF composites, Mater. Sci. Eng. B103 (2003) 140–144.

[3] V.K. Gupta, S. Agarwal, T.A. Saleh, Chromium removal by combining the magnetic properties of iron oxide with adsorption properties of carbon nanotubes, Water Res. 45 (2011) 2207–2212.

[4] T.A. Saleh, V.K. Gupta, Column with CNT/magnesium oxide composite for lead(II) removal from water, Environ. Sci. Pollut. Res. 19 (2012) 1224–1228.

[5] V.K. Gupta, R. Kumar, A. Nayak, T.A. Saleh, M.A. Barakat, Adsorptive removal of dyes from aqueous solution onto carbon nanotubes: a review, Adv. Colloid Interface Sci. 193–194 (2013) 24–34.

[6] X. Xie, L. Gao, Characterization of a manganese dioxide/carbon nanotube composite fabricated using an in situ coating method, Carbon 45 (2007) 2365–2373.

[7] S. Takenaka, T. Arike, H. Matsune, E. Tanabe, M. Kishida, Preparation of carbon nanotube-supported metal nanoparticles coated with silica layers, J. Catal. 257 (2008) 345–355.

[8] C. Gao, W. Li, H. Morimoto, Y. Nagaoka, T. Maekawa, Magnetic carbon nanotubes: synthesis by electrostatic self-assembly approach and application in biomanipulations, J. Phys. Chem. B 110 (2006) 7213–7220.

[9] T. Hayashi, S. Hirono, M. Tomita, S. Umemura, Magnetic thin films of cobalt nanocrystals encapsulated in graphite-like carbon, Nature 381 (1996) 772–774.

[10] J. Wu, L. Kong, High microwave permittivity of multiwalled carbon nanotube composites, Appl. Phys. Lett. 84 (2004) 4956–4958.

[11] G. Korneva, H. Ye, Y. Gogotsi, D. Halverson, G. Friedman, J.C. Bradley, Carbon nanotubes loaded with magnetic particles, Nano Lett. 5 (2005) 879–884.

[12] Mohamed Abdel Salam, Mohamed A. Gabal, Abdullah Y. Obaid, Preparation and characterization of magnetic multi-walled carbon nanotubes/ferrite nanocomposite and its application for the removal of aniline from aqueous solution, Synth. Met. 161 (2012) 2651–2658.

[13] Y. Zhang, M. Zhu, Q. Zhang, H. Yu, Y. Li, H. Wang, Solvothermal one-step synthesis of MWCNTs/Ni$_{0.5}$Zn$_{0.5}$Fe$_2$O$_4$ magnetic composites, J. Magn. Magn. Mater. 322 (2010) 2006–2009.

[14] H. Cao, M. Zhu, Y. Li, J. Liu, Z. Ni, Z. Qin, A highly coercive carbon nanotube coated with Ni$_{0.5}$Zn$_{0.5}$Fe$_2$O$_4$ nanocrystals synthesized by chemical precipitation–hydrothermal process, J. Solid State Chem. 180 (2007) 3218–3223.

[15] F.R. Lamastra, F. Nanni, L. Camilli, R. Matassa, M. Carbone, G. Gusmano, Morphology and structure of electrospun CoFe2O4/multi-wall carbon nanotubes composite nanofibers, Chem. Eng. J. 162 (2010) 430–435.

[16] Q. Zhang, M. Zhu, Q. Zhang, Y. Li, H. Wang, Synthesis and characterization of carbon nanotubes decorated with manganese–zinc ferrite nanospheres, Mater. Chem. Phys. 116 (2009) 658–662.

[17] W. Wang, Q. Li, C. Chang, Effect of MWCNTs content on the magnetic and wave absorbing properties of ferrite-MWCNTs composites, Synth. Met. 161 (2011) 44–50.

[18] A.A. Farghali, M. Bahgat, W.M.A. El Rouby, M.H. Khedr, Decoration of MWCNTs with CoFe$_2$O$_4$ nanoparticles for methylene blue dye adsorption, J. Solution Chem. 41 (2012) 2209–2225.

[19] M.A. Gabal, S. Kosa, T.S. El Muttairi, Magnetic dilution effect of nano-crystalline NiFe2O4 synthesized via sucrose-assisted combustion route, Ceram. Int. 40 (2014) 675–681.

[20] M.A. Gabal, R.S. Al-luhaibi, Y.M. Al Angari, Mn–Zn nano-crystalline ferrites synthesized from spent Zn–C batteries using novel gelatin method, J. Hazard. Mater. 246–247 (2013) 227–233.

[21] Q. Zhang, M. Zhu, Q. Zhang, Y. Li, H. Wang, The formation of magnetite nanoparticles on the sidewalls of multi-walled carbon nanotubes, Compos. Sci. Technol. 69 (2009) 633–638.

[22] M.A. Gabal, R.M. El-Shishtawy, Y.M. Al Angari, Structural and magnetic properties of nano-crystalline Ni–Zn ferrites synthesized using egg-white precursor, J. Magn. Magn. Mater. 324 (2012) 2258–2264.

[23] E. Manova, B. Kunev, D. Paneva, I. Mitov, L. Petrov, C. Estournes, C. D'Orleans, J.L. Rehspringer, M. Kurmoo, Mechano-synthesis, characterization, and magnetic properties of nanoparticles of cobalt ferrite, $CoFe_2O_4$, Chem. Mater. 16 (2004) 5689–5696.

[24] R.D. Waldron, Infrared spectra of ferrites, Phys. Rev. 99 (1955) 1727–1735.

[25] S. Farhadi, M. Zaidi, Bismuth ferrite ($BiFeO_3$) nanopowder prepared by sucrose-assisted combustion method, J. Mol. Catal. A 299 (2009) 18–25.

[26] E.A. Souza, J.G.S. Duque, L. Kubota, C.T. Meneses, Synthesis and characterization of NiO and $NiFe_2O_4$ nanoparticles obtained by a sucrose-based route, J. Phys. Chem. Solids 68 (2007) 594–599.

[27] R. Gimenes, M.R. Baldissera, M.R.A. da Silva, C.A. da Silveira, D.A.W. Soares, L.A. Perazolli, M.R. da Silva, M.A. Zaghete, Structural and magnetic characterization of $Mn_xZn_{1-x}Fe_2O_4$ ($x = 0.2$; 0.35; 0.65; 0.8; 1.0) ferrites obtained by the citrate precursor method, Ceram. Int. 38 (2012) 741–746.

[28] International Union of Pure and Applied Chemistry, IUPAC, Pure Appl. Chem. 57, 1985.

[29] L. Zhou, L. Ji, P. Ma, Y. Shao, H. Zhang, W. Gao, Y. Li, Development of carbon nanotubes/$CoFe_2O_4$ magnetic hybrid material for removal of tetrabromobisphenol A and Pb(II), J. Hazard. Mater. 265 (2014) 104–114.

[30] Y. Lin, X. He, G. Han, Q. Tian, W. Hu, Removal of crystal violet from aqueous solution using powdered mycelial biomass of Ceriporia lacerata P2, J. Environ. Sci. 23 (2011) 2055–2062.

[31] A. Saeed, M. Sharif, M. Iqbal, Application potential of grapefruit peel as dye sorbent: kinetics, equilibrium and mechanism of crystal violet adsorption, J. Hazard. Mater. 179 (2010) 564–572.

[32] S. Lagergren, Zur theorie der sogenannten adsorption gelster stoffe, Kungliga Svenska Vetenskapsakademiens, Handlingar 24 (1898) 1–39.

[33] W. Rudzinski, W. Plazinski, On the applicability of the pseudo-second order equation to represent the kinetics of adsorption at solid/solution interfaces: a theoretical analysis based on the statistical rate theory, Adsorption 15 (2009) 181–192.

[34] Q. Zhang, T. Zhang, T. He, L. Chen, Removal of crystal violet by clay/PNIPAm nanocomposite hydrogels with various clay contents, Appl. Clay Sci. 90 (2014) 1–5.

[35] M.K. Satapathy, P. Das, Optimization of crystal violet dye removal using novel soil-silver nanocomposite as nanoadsorbent using response surface methodology, J. Environ. Chem. Eng. 2 (2014) 708–714.

[36] M.A. Schoonen, M.T. Jan, Schoonen, Removal of crystal violet from aqueous solutions using coal, J. Colloid Interface Sci. 422 (2014) 1–8.

[37] L. Zhang, H. Zhang, W. Guo, Y. Tian, Removal of malachite green and crystal violet cationic dyes from aqueous solution using activated sintering process red mud, Appl. Clay Sci. 93–94 (2014) 85–93.

[38] Y. Lin, X. He, G. Han, Q. Tian, W. Hu, Removal of Crystal Violet from aqueous solution using powdered mycelial biomass of Ceriporia lacerata P, J. Environ. Sci. 23 (2011) 2055–2062.

[39] M. Abdel Salam, Coating carbon nanotubes with crystalline manganese dioxide nanoparticles and their application for lead ions removal from model and real water, Colloids Surf. A 419 (2013) 69–79.

[40] X. Yang, B. Al-Duri, Kinetic modeling of liquid-phase adsorption of reactive dyes on activated carbon, J. Colloid Interface Sci. 287 (2005) 25–34.

[41] A. Kiran Kumar, S. Venkata Mohan, P.N. Sarma, Sorptive removal of endocrine-disruptive compound (estriol, E3) from aqueous phase by batch and column studies: Kinetic and mechanistic evaluation, J. Hazard. Mater. 164 (2009) 820–828.